Mechanisms of Signal Transduction:

Stepped Changes of Monovalent Ligand-binding Force during Ligand-induced Clustering of Integrin $\alpha_{IIB}\beta_3$

Chia-Fen Hsieh, Bo-Jui Chang, Chyi-Huey Pai, Hsuan-Yi Chen, Jin-Wu Tsai, Yung-Hsiang Yi, Yi-Ting Chiang, Da-Wei Wang, Sien Chi, Long Hsu and Chi-Hung Lin

J. Biol. Chem. 2006, 281:25466-25474.
doi: 10.1074/jbc.M601793200 originally published online June 21, 2006

THE JOURNAL OF BIOLOGICAL CHEMISTRY VOL. 281, NO. 35, pp. 25466–25474, September 1, 2006

Stepped Changes of Monovalent Ligand-binding Force during Ligand-induced Clustering of Integrin $\alpha_{IIB}\beta_3$*

Received for publication, February 24, 2006, and in revised form, June 13, 2006 Published, JBC Papers in Press, June 21, 2006, DOI 10.1074/jbc.M601793200

Chia-Fen Hsieh[a1], Bo-Jui Chang[b1], Chyi-Huey Pai[c], Hsuan-Yi Chen[d], Jin-Wu Tsai[a], Yung-Hsiang Yi[a], Yi-Ting Chiang[e], Da-Wei Wang[e], Sien Chi[b,f], Long Hsu[g], and Chi-Hung Lin[a,h,i,j2]

From the [a]Institute of Microbiology and Immunology, National Yang-Ming University, Taipei, Taiwan, the [b]Department of Photonics & Institute of Electro-Optical Engineering, National Chiao-Tung University, Hsinchu, Taiwan, the [c]Institute of Biomedical Sciences, Academia Sinica, Taipei, Taiwan, the [d]Department of Physics, National Central University, Taoyuan, Taiwan, the [e]Institute of Information Science, Academia Sinica, Taipei, Taiwan, the [f]Department of Electrical Engineering, Yuan-Ze University, Taoyuan, Taiwan, the [g]Department of Electrophysics, National Chiao-Tung University, Hsinchu, Taiwan, the [h]Institute of Biophotonic Engineering, National Yang-Ming University, Taipei, Taiwan, the [i]Department of Surgery, Veteran General Hospital, Taipei, Taiwan, and the [j]Division of Medical Research, Taipei City Hospital, Taipei, Taiwan

Recent evidence demonstrated that conformational changes of the integrin during receptor activation affected its binding to extracellular matrix; however, experimental assessment of ligand-receptor binding following the initial molecular interaction has rarely been carried out at a single-molecule resolution. In the present study, laser tweezers were used to measure the binding force exerted by a live Chinese hamster ovary cell that expressed integrin $\alpha_{IIb}\beta_3$ (CHO $\alpha_{IIb}\beta_3$), to the bead carrier coated with the snake venom rhodostomin that served as an activated ligand for integrin $\alpha_{IIb}\beta_3$. A progressive increase of total binding force over time was noticed when the bead interacted with the CHO $\alpha_{IIb}\beta_3$ cell; such an increase was due mainly to the recruitment of more integrin molecules to the bead-cell interface. When the binding strength exerted by a single ligand-receptor pair was derived from the "polyvalent" measurements, surprisingly, a stepped decrease of the "monovalent binding force" was noted (from 4.15 to 2.54 piconewtons (pN)); such decrease appeared to occur during the ligand-induced integrin clustering process. On the other hand, the mutant rhodostomin defective in clustering integrins exhibited only one (1.81 pN) unit binding strength.

Since the early recognition of integrin as an integral membrane complex involved in the trans-membrane association between the extracellular matrix and the cell, integrin heterodimers have been found to play important roles in controlling various steps that regulate processes as diverse as proliferation, development and differentiation, cell migration, and carcinogenesis (1). The initiation of the integrin-mediated activities involves at least two steps, namely, receptor activation and clustering. Taking platelet cells as an example, the integrin $\alpha_{IIb}\beta_3$ proteins on the membrane of a resting platelet bind only loosely to fibrinogen (FBN).[3] Stimulation (or activation) of the platelets with agonists (such as ADP or thrombin) induces an inside-out signaling process that confers on integrin $\alpha_{IIb}\beta_3$ a stronger binding to FBN, resulting in the onset of platelet aggregation. Subsequent integrin clustering triggers complex intracellular signaling pathways that regulate the extent of the irreversible platelet aggregation and clot retraction (2). Using advanced structural biology techniques, several recent reports have provided convincing evidence that indicates the adoption of different molecular conformations by integrin heterodimers when the inside-out signaling pathway is invoked (3–5). Such structural changes are thought to be the mechanisms underlying increased ligand binding by an integrin during the *activation* process. Whether or not ligand binding affinity is further modulated during the subsequent integrin *clustering* process has remained largely elusive (6).

To focus this research on the ligand-receptor interaction during the receptor clustering, we utilized snake venom rhodostomin from *Agkistrodon rhodostoma* as the ligand for integrin $\alpha_{IIb}\beta_3$. Rhodostomin is a member of the disintegrin superfamily (7); it binds very strongly to integrin $\alpha_{IIb}\beta_3$ (8, 9). Unlike the FBN and other extracellular matrix agonists, rhodostomin positively regulates outside-in signaling without prior inside-out activation of integrin $\alpha_{IIb}\beta_3$ (9–11). The structure of rhodostomin has been solved (12). The binding of rhodostomin to the integrin is attributed to its Arg^{49}-Gly^{50}-Asp^{51} (RGD) sequence motif and changing RGD to RGE totally abolishes integrin binding (10). Sequences adjacent to the RGD motif are thought to play regulatory roles; for example, the mutant that has a mutation at Pro^{53} significantly affects the morphogenesis and aggregation activity of rhodostomin on platelets (13).

In this report, we utilize laser tweezers to quantify the bind-

* This work is supported by grants from National Science Council (NSC 94-2627-B-010-004), a grant from Ministry of Education, Aim for the Top University Plan, and Center for Nano-Science and Technology/University System of Taiwan (awarded to C.-H. L.). The costs of publication of this article were defrayed in part by the payment of page charges. This article must therefore be hereby marked "*advertisement*" in accordance with 18 U.S.C. Section 1734 solely to indicate this fact.

[1] These two authors contributed equally to this paper.

[2] To whom correspondence should be addressed: Institute of Microbiology and Immunology, Institute of Biophotonics Engineering, National Yang-Ming University, Taipei, Taiwan. Tel.: 886-2-28267219; Fax: 886-2-28212880; E-mail: linch@ym.edu.tw.

[3] The abbreviations used are: FBN, fibrinogen; Rho-RGD, recombinant wild-type rhodostomin containing $R^{49}G^{50}D^{51}$ motif; Rho-RGE, recombinant mutant rhodostomin containing RGE motif (whose Asp^{51} is substituted by Glu); Rho-P53N, recombinant mutant rhodostomin whose Pro^{53} is substituted by Asn; FAK, focal adhesion kinase; CHO K1, Chinese hamster ovary K1 cell; CHO $\alpha_{IIb}\beta_3$, Chinese hamster ovary K1 cell expressing exogenous integrin $\alpha_{IIb}\beta_3$ proteins; N, newton(s); GCV, generalized cross-validation; MSE, mean square error.

ing force of the interacting ligand-receptor molecular pairs at a single-molecule resolution (usually in a force range of a few pNs) and to monitor the interaction dynamics over time. By focusing a laser beam to a diffraction-limited spot, the laser tweezers technique offers a unique way to manipulate targets and generate molecule-scaled forces (14–16). The use of light also allows the experiments to be performed *in situ* where the biological interactions occur. The measurements so done are much less invasive than techniques such as atomic force microscopy. In the present study, we successfully applied laser tweezers to systemically investigate the binding forces exerted by a live CHO cell that contained integrin $\alpha_{IIb}\beta_3$ on its membrane to a microbead carrier coated with the integrin ligand, rhodostomin. By analyzing the data set that represented the ensemble binding force of more than one ligand-receptor pair (polyvalent), we were able to derive the "unit" binding force, which we believe representing the "monovalent" binding strength between a single molecular pair of rhodostomin and integrin.

EXPERIMENTAL PROCEDURES

Cells and Recombinant Rhodostomin Proteins—The CHO $\alpha_{IIb}\beta_3$ cells were a gift from Dr. Yoshikazu Takada of the Scripps Research Institute (17) and were grown in Dulbecco's modified Eagle's medium supplemented with 10% fetal bovine serum, 0.1 mM non-essential amino acids, 2 mM L-glutamine, and 50 μM G418 (Invitrogen). CHO $\alpha_{IIb}\beta_3$ cells were incubated in 5% CO_2 at 37 °C. The rhodostomin gene was a gift from Dr. SJ Lo of Chang-Gung University, Tao-Yuan, Taiwan. The parental CHO K1 cells, which contained no integrin $\alpha_{IIb}\beta_3$, were purchased from ATCC and grown in F-12 medium supplemented with 10% fetal bovine serum, 0.1 mM non-essential amino acids. Generation and purification of the recombinant rhodostomin proteins were done according to a previous report (18). All beads used in this study were polystyrene beads (Bangs Laboratories); the coating with recombinant rhodostomin proteins was done by the hydrophobic adsorption method (19). Essentially, beads were incubated with 10 μg/ml proteins in phosphate-buffered saline at 4 °C overnight with gentle mixing, washed with phosphate-buffered saline for three times, and further blocked with 5% heat-treated bovine serum albumin at 4 °C for 2 h.

Cell Adhesion Assay—The cell adhesion assay was performed as described previously (20, 21). The adhesion substrates were coated with different concentrations of recombinant rhodostomin as indicated at 37 °C for 2 h, followed by 1% heat-treated bovine serum albumin at 4 °C overnight. CHO $\alpha_{IIb}\beta_3$ and parental CHO K1 cells were harvested and then plated on the substrates at the density of 5×10^4 cells/well at 37 °C for 30 min. The cells that remained adhering to the substrate after a standard wash procedure were determined by the methylthiazolyldiphenyltetrazolium bromide assay. Absorbance was read at 570 nm.

Focal Adhesion Kinase (FAK) Phosphorylation Assay—The FAK phosphorylation experiments were done according to the method described previously (22). Briefly, cells were incubated with 100 μg/ml recombinant rhodostomin proteins, fibrinogen, or mock solution for 30 min, then lysed and immunoprecipitated with anti-FAK antibodies (Upstate Biotechnology). The resulting immuno-complexes were blotted with anti-FAK and anti-phosphotyrosine antibodies (Upstate Biotechnology) and detected by the chemiluminescence assay (PerkinElmer Life Sciences).

Immunofluorescence Staining—Immunofluorescence staining was done as described previously (22). Briefly, suspended cells were incubated with 200 μg/ml Rho-RGD, Rho-P53N, or mock solution for 30 min, then fixed, permeabilized, and labeled with monoclonal antibodies made against human integrin β_3 or integrin α_{IIb} (Chemicon), followed by fluorochrome-conjugated secondary antibodies. The resulting slides were observed using a Leica TCS SP2 confocal microscope and a Leica DM IRBE epifluorescence microscope.

Laser Tweezers Construction—The assembly of laser tweezers was done in the laboratory (23, 24). A 100-milliwatt CW TEM_{00} mode diode laser at $\lambda = 830 \pm 10$ nm (JDS Uniphase Corp.) was used for trapping; the power was controlled by LabVIEW (National Instrument) through a current driver (Newport). A probing He-Ne laser (JDS Uniphase Corp.) was also directed to the trapped object to generate a forward scattering image which was used to better position or monitor the displacement of the trapped object.

Trapping Force Calibration—The dragging force method was applied to calibrate the trapping force of the laser tweezers. The trapping force of the laser tweezers exerted on the bead positioned at the 2 μm off-center position (in the ΔP mode measurements) was measured and calculated using the modified form of Stoke's Law,

$$f = \frac{6\pi\eta\nu r}{1 - \frac{9}{16}\left(\frac{r}{h}\right) + \frac{1}{8}\left(\frac{r}{h}\right)^3 - \frac{45}{256}\left(\frac{r}{h}\right)^4 - \frac{1}{16}\left(\frac{r}{h}\right)^5} \quad \text{(Eq. 1)}$$

where η was the viscosity of the medium, ν was the velocity of the laminar flow, r was the radius of the polystyrene bead (3.75 μm), and h was the distance of the trapped bead from the wall of laminar flow. The maximum and minimum trapping forces of laser tweezers at the 2 μm off-center position are 21 and 1.5 pN, respectively.

Force Measurements: the ΔT and ΔP Mode—Binding force measurements between the bead and the cell were done in two ways, the ΔT and ΔP modes (Fig. 3*A*). In the ΔT mode, a bead was guided to contact a cell. After a certain interaction period (ΔT; from 10 to 100 s in a 10-s increment), a constant force (21 pN) was applied to hold the bead while the cell was moved away from the trapped bead by the motorized stage at a constant velocity of 1 μm/s. The percentage of the beads that resisted such detaching manipulation was plotted as a function of ΔT (Fig. 3*B*). In the ΔP mode, the range of the binding force distribution after a fixed period of molecular interaction was determined. A bead was held in contact with a cell by laser tweezers for 40 s (in Rho-RGD bead experiments) or 80 s (in Rho-P53N bead experiments). The laser trap was turned off and displaced off the bead-center by 2 μm. The laser was then turned on and increased the power at a steady rate (the loading rate of the trapping force is estimated 1.74 pN/s). The bead was released then retrapped twice; the min-

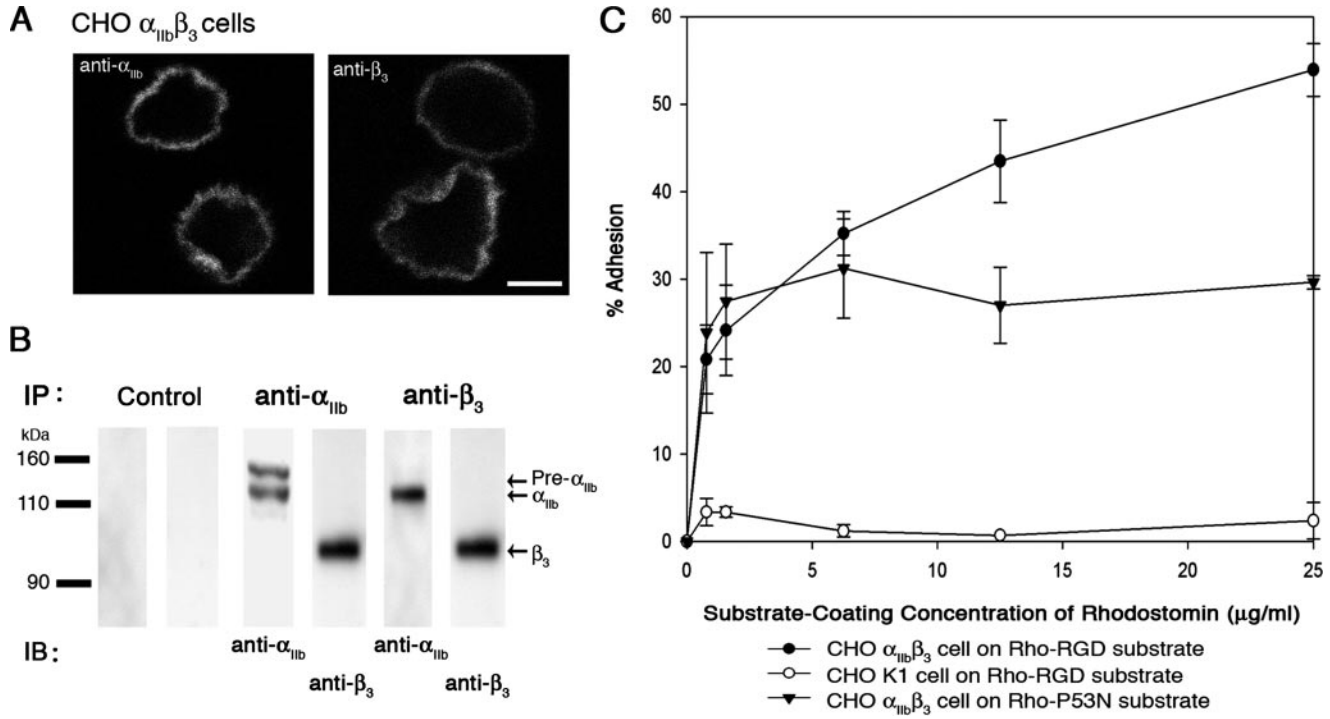

FIGURE 1. **Recombinant rhodostomin proteins interact with CHO$\alpha_{IIb}\beta_3$ cells without the need of prior activation.** *A*, immunofluorescence staining demonstrates that the exogenously engineered integrin α_{IIb} and integrin β_3 proteins are both present on the plasma membranes of CHO $\alpha_{IIb}\beta_3$ cells. *Scale bar*, 8 μm. *B*, the presence of integrin α_{IIb} in the immunoprecipitates of anti-integrin β_3, and vice versa, suggests that both subunits form heterodimers in CHO $\alpha_{IIb}\beta_3$ cells. *C*, the cell adhesion assay: CHO $\alpha_{IIb}\beta_3$ cells adhered to Rho-RGD (*close circles*) and Rho-P53N (*close triangles*) at different substrate coating concentrations, but the parental CHO K1 cells (*open circles*) did not adhere to Rho-RGD at any substrate coating concentration. Each data point represents the mean ± S.D. of triplicate experiments.

imal force just enough to "retrap" the bead was recorded. All the adjustments mentioned above were automated by computer program.

Statistical Analysis—The data set of the ΔP mode experiments (Figs. 4 and 5) were subjected to statistical analyses starting with non-parametric methods, including generalized cross-validation (GCV)-Loess (25, 26) method, GCV-Spline method, minimal frequency selection, and maxima frequency selection method. In essence, the entire data set was first viewed as a continuous process and then categorized into separate groups by dichotomizing the length of duration (the distance between the means of groups) without making any assumption. The best optimization was determined by equality of durations and tested by the nonparametric Willcoxon rank sum test under the "obeying small sample size" hypothesis. From the non-parametric results, a hypothetical (grouping) model was built up, which was then subjected to the parametric (p-median) analysis (27). The significance level was set at $p < 0.1$. All statistical analyses were performed by Microsoft EXCEL and SAS 8.2 versions.

RESULTS

Recombinant Rhodostomins Specifically Interact with Integrin $\alpha_{IIb}\beta_3$ Expressed on CHO $\alpha_{IIb}\beta_3$ Cells—Both integrin α_{IIb} and β_3 genes were co-transfected to CHO K1 cells that contained no endogenous integrin $\alpha_{IIb}\beta_3$ protein of their own. As shown in Fig. 1*A*, the resulting CHO $\alpha_{IIb}\beta_3$ cells contained the exogenous proteins on the plasma membranes when visualized by immunofluorescence staining. Immunoprecipitation experiments (Fig. 1*B*) demonstrated that integrin α_{IIb} was present in the immunocomplexes "pulled down" by the anti-integrin β_3 antibody, and vice versa, suggesting that indeed the two subunits formed heterodimers in CHO $\alpha_{IIb}\beta_3$ cells.

When plated a surface coated with the wild-type rhodostomin (Rho-RGD), CHO $\alpha_{IIb}\beta_3$ cells adhered tightly to the substrate in a dose-dependent manner (*closed circles*, Fig. 1*C*). In contrast, the parental CHO K1 cells adhered poorly to the Rho-RGD substrate (*open circles*) and neither did the substrate that coated with mutant rhodostomin whose RGD domain had been changed to RGE (Rho-RGE) support the adhesion of CHO $\alpha_{IIb}\beta_3$ cells (data not shown). These results indicated that the adhesion of CHO $\alpha_{IIb}\beta_3$ cells to the rhodostomin substrate was mediated by the interactions between the rhodostomin ligand and the integrin $\alpha_{IIb}\beta_3$ proteins. Interesting results were noticed when the CHO $\alpha_{IIb}\beta_3$ cells were plated on the substrate coated with the mutant rhodostomin whose proline (Pro^{53}) had been changed to asparagine (Rho-P53N) (*closed triangles*). At low concentrations (<6.25 μg/ml), the Rho-P53N substrates supported the adherence of CHO $\alpha_{IIb}\beta_3$ cells almost equally good as the wild-type Rho-RGD. Increased coating of Rho-P53N did not further increase the cell adherence. In fact, at 25 μg/ml, only about half of the cell adhesion was observed in the Rho-P53N group, compared with Rho-RGD. This finding suggested that certain promoting effects (on cell adhesion) elicited by the wild type rhodostomin were disrupted by the P53N mutation, although the initial binding event appeared to remain intact.

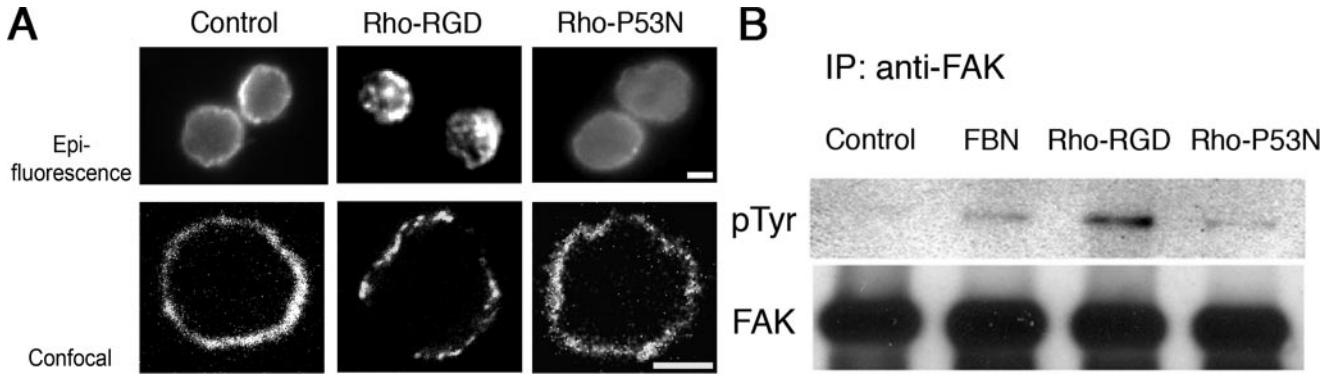

FIGURE 2. **Ineffectiveness of Rho-P53N in clustering integrin $\alpha_{IIb}\beta_3$ and phosphorylating FAK.** *A*, CHO $\alpha_{IIb}\beta_3$ cells were treated with mock solution (*control*), wild-type Rho-RGD, or mutant Rho-P53N proteins and immunostained with anti-β_3 antibody. Immunofluorescence results in the *three upper panels* were observed with an epifluorescence microscope and in the *three lower panels* were observed with a confocal microscope. Only exposure to Rho-RGD elicited a significant integrin $\alpha_{IIb}\beta_3$ clustering pattern. *Scale bar*, 8 μm. *B*, CHO $\alpha_{IIb}\beta_3$ cells were treated with mock solution (*control*), FBN, wild-type Rho-RGD, or mutant Rho-P53N proteins, immunoprecipitated with anti-FAK antibody, and immunoblotted with anti-FAK and anti-phosphorylated tyrosine (pTyr) antibody. Only exposure to Rho-RGD elicited a significant increase in FAK phosphorylation. Since integrin clustering is prerequisite for FAK phosphorylation, these results indicate that only Rho-RGD could induce effective clustering of integrin $\alpha_{IIb}\beta_3$ in CHO $\alpha_{IIb}\beta_3$ cells.

Ineffectiveness of Rho-P53N Mutant in Clustering Integrin $\alpha_{IIb}\beta_3$ and Triggering Downstream Signaling—Since the cell adhesion is regulated initially by ligand-receptor binding and further enhanced by receptor clustering. We tested whether the mutant rhodostomin Rho-P53N was defective in clustering integrin or in triggering the downstream signaling. As shown in Fig. 2*A*, integrin $\alpha_{IIb}\beta_3$ proteins were evenly distributed on the cell membrane of a control CHO $\alpha_{IIb}\beta_3$ cell. After the addition of soluble Rho-RGD to the cell for 30 min, a patchy integrin $\alpha_{IIb}\beta_3$ pattern was revealed under both an epifluorescence microscope and a confocal microscope. In contrast, treatments with the Rho-P53N mutant failed to cause any integrin clustering or membrane patch formation. Since integrin clustering has been shown to trigger the occurrence of downstream tyrosine phosphorylation (*pTyr*) of FAK (28), we set up experiments to examine the level of FAK phosphorylation following various ligand treatments. As shown in Fig. 2*B*, treating CHO $\alpha_{IIb}\beta_3$ cells with FBN caused only little FAK phosphorylation, since most of the cellular integrin $\alpha_{IIb}\beta_3$ proteins were not activated (and therefore could not be clustered). On the other hand, exposure of the CHO $\alpha_{IIb}\beta_3$ cells to wild-type Rho-RGD was enough to cause a very significant increase of FAK phosphorylation, while treating the same cells with the mutant Rho-P53N had only a minor effect. These results indicated that mutant Rho-P53N was less effective than the wild-type Rho-RGD in clustering integrin $\alpha_{IIb}\beta_3$ and was unable to trigger the downstream signaling processes.

A Typical Ensemble Interaction between Rhodostomin and Integrin Was Characterized by a Progressive Increase in Total Binding Force Over Time—In addition to the biochemical methods, we utilized laser tweezers to measure the binding strength between the rhodostomin bead and the CHO $\alpha_{IIb}\beta_3$ cell. As described under "Experimental Procedures," the binding force between the bead and the cell could be measured by either ΔT or ΔP assay (Fig. 3*A*). The ΔT assay was designed to quantify the dynamic change of the total binding force over time. The beads were held to contact with the CHO $\alpha_{IIb}\beta_3$ cells for a fixed interaction period; the percentage of the bead (30 measurements for each curve, three repeats) that remained bound to the cells (or resisted the 21-pN detaching force) was determined. As shown in Fig. 3*B*, the percentage of bound bead progressively increased in the first 50 s of interaction then reached a plateau (*closed circles*). There was not significant binding between Rho-RGE bead and the CHO $\alpha_{IIb}\beta_3$ cell (*open circles*). The binding of Rho-P53N beads (*closed triangles*) increased much slower than the wild-type Rho-RGD beads and never reached plateau even after a 10 min interaction period (data not shown). Furthermore, neither the Rho-RGD bead, nor the Rho-P53N bead could bind to the parental CHO K1 cells (data not shown). These control experiments indicated that the bead-cell interactions studied here were mediated by the rhodostomin protein on the bead and the engineered integrin $\alpha_{IIb}\beta_3$ on the CHO $\alpha_{IIb}\beta_3$ cell.

Quantification of the Trapping Force Exerted by the Laser Tweezers—To perform the ΔP experiments, we need to first calibrate the trapping force exerted by the laser tweezers. As shown in Fig. 3*C*, we first determined that the output of laser illumination power was in a stable linear relationship to the input current and such linear relationship was maintained over a wide range of current-loading rates (30, 3, and 0.3 mA/s) and that the illumination output responded almost instantaneously to the change of the input current. We then measured the actual trapping force by using the drag force assay (29). From these calibrations, we determined that the trapping force exerted by our system could range from 1.5 to 21 pN. When the "trapping force" (in pN) is plotted as a function of laser current (mA), a linear relationship with a slope of 0.58 pN/mA was found (R^2 = 0.9812; Fig. 3*D*). The force was limited by the 100-milliwatt diode laser employed here.

Two Monovalent Binding Forces Were Derived from the Ensemble Measurements of the Bead-Cell Interactions Using Wild-type Rhodostomin—The binding force exerted by a single Rho-RGD bead and a CHO $\alpha_{IIb}\beta_3$ cell was determined after a 40-s interaction period by the ΔP experiment (see Fig. 3*A* and "Experimental Procedures"). The histogram of 210 measurements is shown in Fig. 4*A*. Increase of the interaction period made the histogram shift to the right, while the decrease of the interaction period made the pattern shift to the left (data not

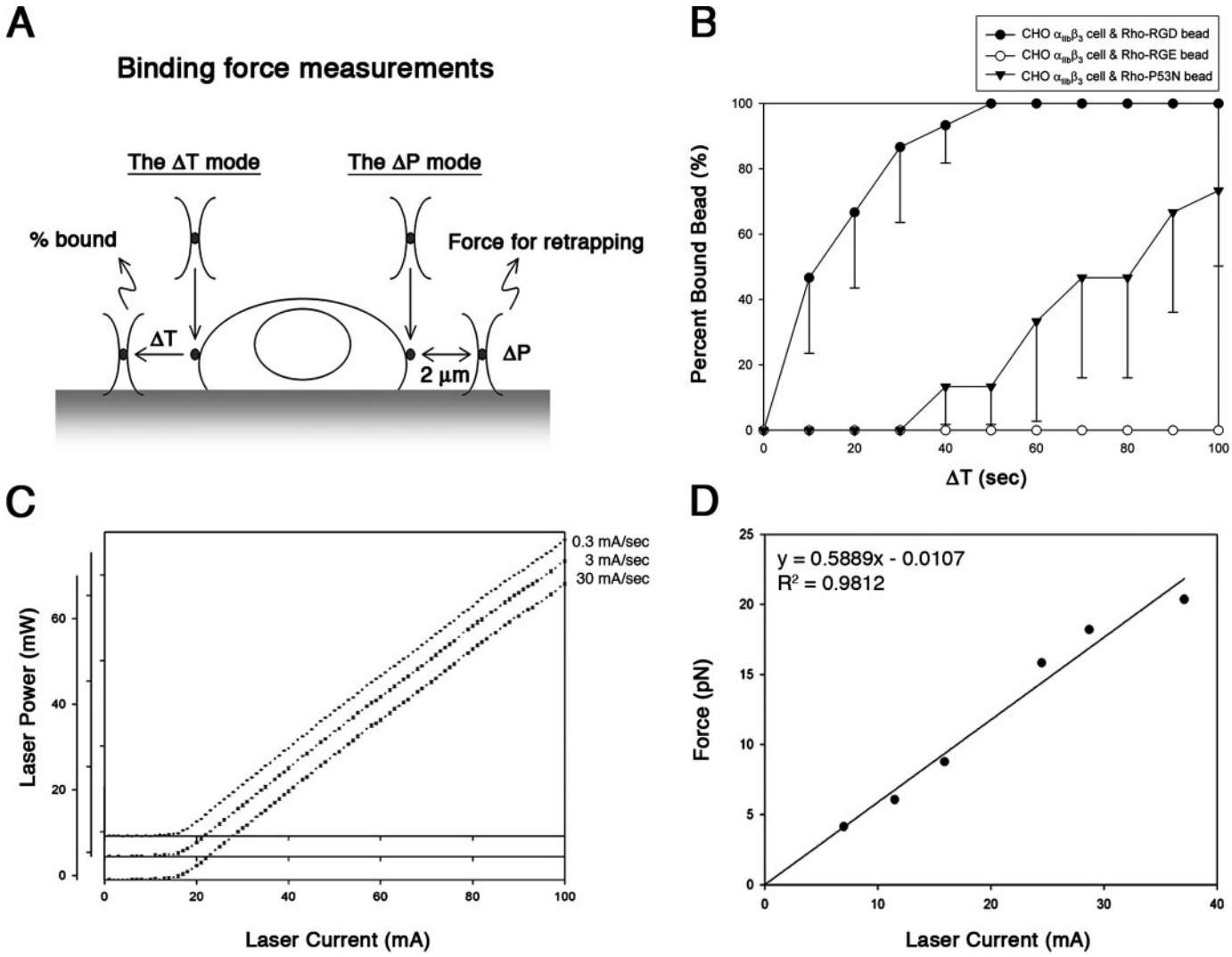

FIGURE 3. **Calibrations and applications of laser tweezers.** *A*, the binding force measurements are performed by either the ΔT or ΔP method (see "Experimental Procedures." *B*, ΔT mode force measurement. Rho-RGD coated beads (*close circles*) reach binding plateau within 50 s of bead-CHO $\alpha_{IIb}\beta_3$ cell interaction. Rho-P53N-coated beads exhibited a much slower increase binding interaction with CHO $\alpha_{IIb}\beta_3$ cell (*close triangles*). There was no binding between Rho-RGE coated beads and parental CHO $\alpha_{IIb}\beta_3$ cells (*open circles*). Thirty measurements were done for each curve and the mean ± S.D. for each is shown (three repeats). *C*, calibration of laser illumination power by input current. Note the linear relationship between 21 and 100 mA input current was maintained over a wide range of current-loading rates (from 0.3, 3, to 30 mA/s). Ten experiments were done for each data point and the mean ± S.D. for each is shown. *D*, calibration of trapping force by laser illumination current. Five separate experiments were done. A linear relationship with a slope of 0.58 pN/mA was found ($R^2 = 0.9812$).

shown). Moreover, the histogram pattern suggested a distribution with several clusters (or groups). To test whether such a non-random pattern is a feature of the entire data set, or simply reflected insufficient sampling, we analyzed the data accumulation trend as the sample size increased. As shown in Fig. 4*B*, the pattern of cumulative data taken from 25, 50, or 75 measurements were very different. When the measurements exceeded 100, the cumulative plots appeared to reach a very significant overlap, indicating that the experimental measurements performed here ($n = 210$), and the features obtained from this sampling could well represent the entire data set.

To further analyze the grouping of the histogram, we applied a series of non-parametric statistical methods to first view the histogram as a continuous process and then categorized it into separate groups without making any assumption. As shown in Fig. 4*C*, we first performed local regression to smooth the relationship between the force and the event frequency using GCV-Loses methods. In this test, different curve fittings were applied using different local regression values, such as rolling averages of 5, 15, and 25% of the neighboring data (*cyan*, *orange*, and *purple curves*, respectively). Note that the 5% local regression plot demonstrated the best fit, which transformed the original dataset into a series of regular event containing seven peaks ($R^2 = 0.745$, MSE = 5.48). Similar conclusions were made using GCV-Spline methods. In another approach (minimal frequency selection method), we selected from the raw histogram what appeared to be least frequent data as compared with its adjacent data points. When these low frequency data points were used to segregate the entire histogram data set, we found again seven separate groups: (4.977, 5.230), (8.011, 8.264, 8.516), (10.033, 10.539), (12.308, 12.561), (14.836, 15.089, 15.342), (17.364, 17.617), and (20.398). The same kind of group-

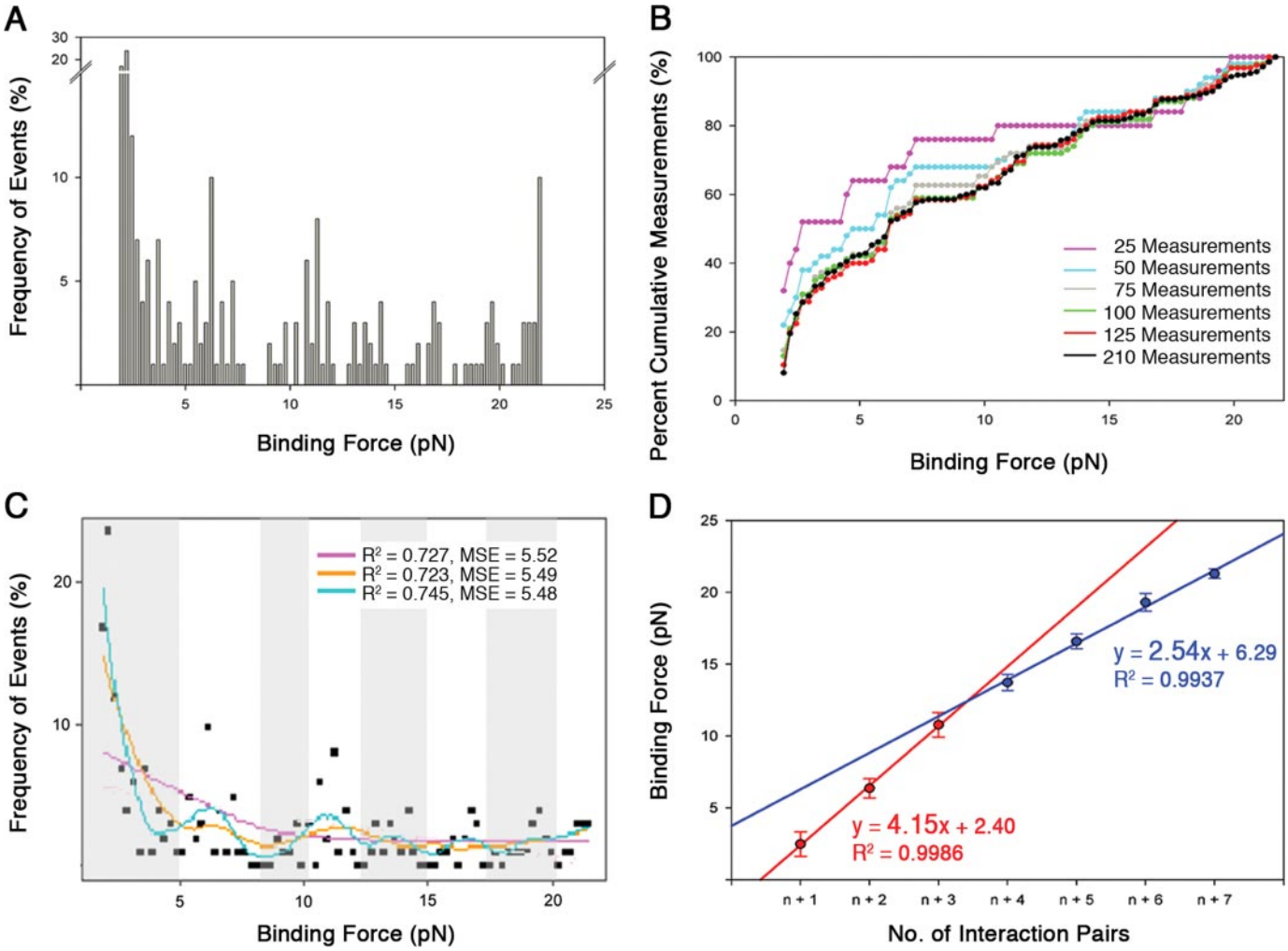

FIGURE 4. **Two monovalent ligand-binding forces are derived from Rho-RGD bead-CHO$\alpha_{IIb}\beta_3$ cell interactions.** *A*, the histogram plot shows the frequency of events as a function of binding force. $n = 210$ measurements. *B*, the data cumulative plot demonstrates increased similarity in the trend of data accumulation as the sample sizes increase (from 25, 50, 75, 100, 125, to 210 measurements, color-coded lines). More than 100 measurements are considered representative of the data set. *C*, non-parametric analyses using GCV-Loses method. The original data points shown in Fig. 3*A* are presented as *filled squares*, together with the resulting 5% local regression curve are shown (*cyan line*, $R^2 = 0.745$, MSE = 5.48). Local regressions based on 15% (*orange line*) and 25% (*purple line*) neighboring data are also shown. From the non-parametric analyses, the histogram data series are grouped into seven sectors (*alternately shaded areas*). *D*, mean ± S.D. within each sector was calculated and plotted as a function of numbers of interacting molecular pairs. Based on Willcoxon rank sum test, two sets of durations (*blue* and *red lines*) could be identified ($p < 0.1$).

ing was made if the maximal frequency selection method was applied.

Based on such non-parametric analyses, 7 sectors could be identified (as *alternative shadings* in Fig. 4*C*). The mean and S.D. of the data points within each sector were then calculated. They were (in pN): 2.486 ± 0.850, 6.368 ± 0.668, 10.784 ± 0.851, 13.730 ± 0.561, 16.587 ± 0.510, 19.302 ± 0.624, 21.294 ± 0.327; these values were plotted as a function of numbers of molecular pairs involved in the binding (n, $n+1$, $n+2$, $n+3$ etc.; Fig. 4*D*). Note that the very similar s.d. values and durations (*i.e.* the differences between means of neighboring sectors, which were averaged 3.15 pN), were consistent with the notion that there was a unit binding force present in the system. Using the Willcoxon rank sum test, we further noticed that the mean ± S.D. values shown in Fig. 4*D* could be best separated into two groups (*red line* at $R^2 = 0.9986$ and *blue lines* at $R^2 = 0.9937$, $p = 0.0542$). The first three durations were separated by a unit of 4.15 pN and last four durations by a unit of 2.54 pN.

We then performed the parametric analyses using partition around medoids (also known as p-median methods (27)) to identify the clustering sectors. Random grouping was first set with each group represented by the center point. The quality of clustering was indicated by the sum of the distance between the center point and another closest center. The solution to the p-median problem is to set the p center so the total distance could be minimized. We implemented a dynamic computer program to solve the p-median problem using p values from 2 to 15. The results revealed that $p = 7$ was a sensible choice, since the reduction in the total distance by adding one more clustering group ($p = 8$) was not significant. The means of the seven sectors grouped by the p-median method were (in pN): 2.234, 3.731, 6.328, 10.784, 13.730, 16.678, and 20.236. There was again a large duration (4.01 pN) across the first three means and a small duration (2.50 pN) across the last four means; these durations were comparable with those obtained by the non-parametric methods described above (4.15 and 2.54 pN).

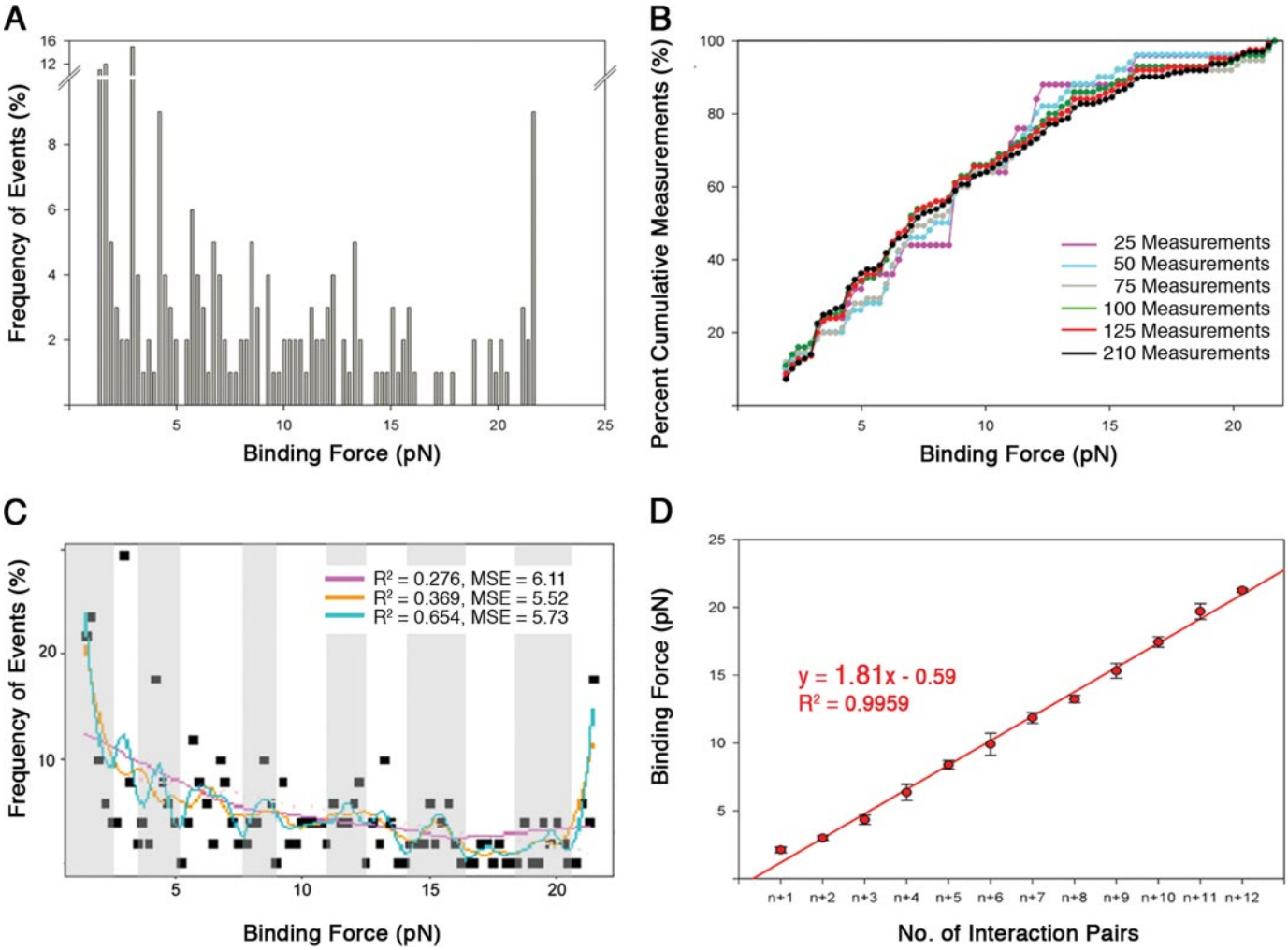

FIGURE 5. **Only one monovalent binding force was derived from Rho-P53N bead-CHO$\alpha_{IIb}\beta_3$ cell interactions.** *A*, the histogram plot showing the frequency of events as a function of binding force; $n = 176$ measurements. *B*, cumulative data plot indicates that >100 measurements are adequate to represent the data set. *C*, non-parametric analysis of the histogram data series using GCV-Loses method. Original data points shown in Fig. 4*A* are presented as *filled squares* together with the resulting 5% local regression curve are shown (*cyan line*, $R^2 = 0.654$, MSE = 5.73). Local regression curves based on 15% (*orange line*) and 25% (*purple line*) neighboring data are also shown. These data series can be grouped into 12 sectors (*alternately shaded areas*). *D*, mean ± S.D. within each sector is calculated and plotted as a function of numbers of interacting molecular pairs. Based on Willcoxon rank sum test, there is only one duration.

Only One Monovalent Binding Force Was Derived from the Ensemble Measurements of the Bead-Cell Interactions Using the P53N Rhodostomin Mutant—Similar experiments and statistical procedures were applied to analyze the binding force histogram obtained from the interactions of the Rho-P53N bead and the CHO $\alpha_{IIb}\beta_3$ cell (Fig. 5). Since the binding of Rho-P53N to integrin $\alpha_{IIb}\beta_3$ was much weaker than Rho-RGD, the bead-cell interaction period was extended to 80 s, as compared with 40 s used in the wild-type rhodostomin (Rho-RGD) experiments. A total of 176 measurements were made and their histogram is shown in Fig. 5*A*. The data accumulation pattern suggested that such a sampling size was enough to represent the entire data set (Fig. 5*B*). The GCV-Loses smooth plot supported the use of 5% local regression curve (*cyan curve*) with $R^2 = 0.654$, MSE = 5.73 (Fig. 5*C*) and led to the grouping into 12 sectors (*alternative shadings* in Fig. 5*C*). In Fig. 5*D*, the plot of mean ± S.D. values revealed only one single duration of 1.81 pN. Subsequent parametric *p*-median analyses reached a similar conclusion of a 12-sector grouping and the presence of a single duration of 1.77 pN.

DISCUSSION

The increase in monovalent ligand binding by an integrin heterodimer during the activation phase is well documented; it is less clear if and how further modulations of ligand binding take place during the receptor clustering phase (30, 31). One of the most striking findings of this report is the identification of two different "monovalent binding forces" during the rhodostomin-induced clustering of the integrin $\alpha_{IIb}\beta_3$ receptors. From the results shown in Fig. 4*D*, it appears that the high monovalent binding force (4.15 pN) is likely associated with the interaction that involves a lower number of molecular pairs, while the low monovalent binding force (2.54 pN) is derived from data involving more molecular pairs. These results suggest strongly that the activated integrin receptor exhibits high binding strength at the initial or early phase of interaction with the ligand. When more ligand-receptor pairs participate in such interaction, as may occur during the receptor-clustering phase, the total binding effectively increases (due to the polyvalence), while the monovalent binding force contributed by the

individual ligand-receptor pair actually decreases. Of course this conclusion is an inference based on the current experimental data. Further independent measures of the unit binding force are needed.

The rhodostomin-coating procedures employed here allowed a very low density of ligand on the bead surface such that only a few ligand-receptor interactions were actually measured. In the experiments shown in Figs. 4 and 5, there were originally ~2,000 measurement attempts; however, only <10% of them (210 in Fig. 4 and 176 in Fig. 5) are "informative," while the majority of the beads either fail to bind to the cell or only exhibit <1.5 pN binding strength (the minimal reliable trapping force exerted by our laser tweezers) and were not included in the statistic analysis. We believe that to limit the number of interacting pairs being quantified are essential for deriving the monovalent binding force from the ensemble measurements, otherwise the force distribution histogram would become too complicated to analyze. When the bead-cell interaction time increases, the force distribution (as the one shown in Fig. 4*A* or 5A) significantly shifts to the right, while decrease of the interaction time makes the pattern shift to the left (data not shown).

The binding strength and the function to trigger downstream signaling are very different between the wild-type rhodostomin and the Rho-P53N mutant. It takes twice as much interaction time to obtain the force distribution histogram shown in Fig. 5 than the wild-type rhodostomin shown in Fig. 4. Rho-RGD can support adhesion of CHO $\alpha_{IIb}\beta_3$ cells and form large integrin patch when add to the medium. It could also effectively trigger tyrosine phosphorylation of FAK. On the other hand, the Rho-P53N mutant supports only basic cell adhesion function but never reach the same level of cell adhesion potency as the wild-type protein. Soluble Rho-P53N causes no integrin clustering or patch formation and does not elicit FAK phosphorylation (Figs. 1 and 2). The total binding strength between Rho-P53N and integrin $\alpha_{IIb}\beta_3$ increases in a much slower rate and never reaches the plateau as the wild-type rhodostomin (Fig. 3*B*). To link these differences in functions to their difference in possessing two or one monovalent binding unit, we reason that Rho-P53N (and maybe other mutations surrounding the RGD integrin-binding motif) may lose the ability to further strengthen the binding between the ligand-receptor pair or to effectively trigger downstream events of integrin signaling.

The presence of two monovalent binding forces is not due to the involvement of the other endogenous integrin heterodimers of the CHO $\alpha_{IIb}\beta_3$ cells or nonspecific binding force, since neither Rho-RGD nor Rho-P53N exhibits any binding interaction with the parental CHO K1 cell. It is unlikely that the rupture force measured in our system resulted from the separation of ligands from the polystyrene beads, because the nonspecific adsorption force between proteins and the polystyrene bead is greater than 100 pN, which is several orders of magnitude greater than monovalent binding force derived here (32, 33). We have also carefully ruled out the possibility that membrane tether formation takes place in our measurements (data not shown).

The monovalent binding force derived here are comparable with previous data using micropipette method (34) to measure FBN-integrin $\alpha_{IIb}\beta_3$ binding, which reported a unit binding force of 2.1 pN for antibody-activated integrin $\alpha_{IIb}\beta_3$ and 0.57 pN for the inactivated integrin. In another series of study using laser tweezers with a force loading rate of 200 pN/s, Arya *et al.* (35) demonstrated a unit force between FBN and integrin $\alpha_{IIb}\beta_3$ to be 2.4 pN for inactivated integrin and 6.3 pN for the $MnCl_2$-activated integrin. Note that the unit binding force derived from these measurements ((34) (35) and this study) are much smaller than the single FBN-integrin $\alpha_{IIb}\beta_3$ bond strength reported by Litvinov *et al.* (80 ~ 100 pN; Ref. 36). The difference may result from the different types of cell models (CHO cell *versus* platelets), different force loading rates (<200 pN/s *versus* 20,000 pN/s), as well as the possible involvement of membrane tether.

Taken together, we propose the following mechanisms when a ligand encounters an activated integrin. An activated integrin binds tightly to the ligand; such high affinity is essential to initiate the interaction with the ligand. Subsequent clustering of the receptors then enables the polyvalent binding. Although the total binding strength increases over time (due mainly to the recruitment of more interacting molecular pairs), the monovalent binding contributed by individual molecular pair actually decreases. In support of this model, recent evidence has revealed two conformations that are adopted by activated integrin $\alpha_{IIb}\beta_3$ in CHO cells (3). The high affinity form initiated platelet function but is energy unfavorable. Platelet cells solve this energy hurdle by adopting the low affinity or energy favorable form during the later (clustering) phase of the ligand-receptor interaction (37). The nature of the underlying observed stepped reduction of monovalent binding force is currently unknown but could be due to further conformational changes of the integrin (38), signaling complex formation, the interactions with the cytoskeleton (39–41), or the combination of all.

Acknowledgments—We thank Dr. Szecheng J. Lo for offering rhodostomin constructs, Dr. Yoshikazu Takada for CHO cells, and Weber Chen for technical support. Drs. Arthur E. Chiou of National Yang-Ming University and Ernst Stelzer of EMBL helped the setup of laser tweezers. Drs. Liu Ting-Ting, Chia-Lin Ho, I-Ching Hsiao, and Yann-Jang Chen provided insightful thoughts throughout this research.

REFERENCES

1. Mould, A. P., and Humphries, M. J. (2004) *Curr. Opin. Cell Biol.* **16,** 544–551
2. Payrastre, B., Missy, K., Trumel, C., Bodin, S., Plantavid, M., and Chap, H. (2000) *Biochem. Pharmacol.* **60,** 1069–1074
3. Takagi, J., Petre, B. M., Walz, T., and Springer, T. A. (2002) *Cell* **110,** 599–611
4. Vinogradova, O., Velyvis, A., Velyviene, A., Hu, B., Haas, T., Plow, E., and Qin, J. (2002) *Cell* **110,** 587–597
5. Carman, C. V., and Springer, T. A. (2003) *Curr. Opin. Cell Biol.* **15,** 547–556
6. van Kooyk, Y., and Figdor, C. G. (2000) *Curr. Opin. Cell Biol.* **12,** 542–547
7. Huang, T. F., Wu, Y. J., and Ouyang, C. (1987) *Biochim. Biophys. Acta.* **925,** 248–257
8. Chang, H. H., Lin, C. H., and Lo, S. J. (1999) *Exp. Cell Res.* **250,** 387–400
9. Chang, H. H., and Lo, S. J. (1998) *Toxicon* **36,** 1087–1099
10. Chiang, H. S., Yang, R. S., and Huang, T. F. (1995) *Br. J. Cancer* **71,** 265–270
11. Sun, D. S., Lo, S. J., Lin, C. H., Yu, M. S., Huang, C. Y., Chen, Y. F., and

Chang, H. H. (2005) *J. Biomed. Sci.* **12,** 321–333
12. Adler, M., Lazarus, R. A., Dennis, M. S., and Wagner, G. (1991) *Science* **253,** 445–448
13. Chang, C. P., Chang, J. C., Chang, H. H., Tsai, W. J., and Lo, S. J. (2001) *Biochem. J.* **357,** 57–64
14. Ashkin, A. (1970) *Phys. Rev. Lett.* **24,** 156–159
15. Ashkin, A., Dziedzic, J. M., Bjorkholm, J. E., and Chu, S. (1986) *Opt. Lett.* **11,** 288–290
16. Sheetz, M. P. (1999) *Laser Tweezers in Cell Biology*, pp. 1–25, Academic Press, San Diego, CA
17. O'Toole, T. E., Loftus, J. C., Du, X. P., Glass, A. A., Ruggeri, Z. M., Shattil, S. J., Plow, E. F., and Ginsberg, M. H. (1990) *Cell Regul.* **1,** 883–893
18. Chang, H. H., Tsai, W. J., and Lo, S. J. (1997) *Toxicon* **35,** 195–204
19. Cantarero, L. A., Butler, J. E., and Osborne, J. W. (1980) *Anal. Biochem.* **105,** 375–382
20. Mekrache, M., Kieffer, N., and Baruch, D. (2002) *Br. J. Haematol.* **116,** 636–644
21. Larrucea, S., Gonzalez-Manchon, C., Butta, N., Arias-Salgado, E. G., Shen, L., Ayuso, M. S., and Parrilla, R. (2002) *Blood* **99,** 2819–2827
22. Li, R., Mitra, N., Gratkowski, H., Vilaire, G., Litvinov, R., Nagasami, C., Weisel, J. W., Lear, J. D., DeGrado, W. F., and Bennett, J. S. (2003) *Science* **300,** 795–798
23. Lin, C. H., and Forscher, P. (1995) *Neuron* **14,** 763–771
24. Tsai, J. W., Liao, B. Y., Huang, C. C., Hwang, W. L., Wang, D. W., Chiou, A., and Lin, C. H. (2000) *Proc. SPIE* **4082,** 213–221
25. Cleveland, W. S. (1979) *J. Am. Statist. Assoc.* **74,** 829–836
26. Cleveland, W. S., Devlin, S. J., and Grosse, E. (1998) *J. Econometr.* **37,** 87–114
27. Kaufman, L., and Rousseeuw, P. J. (1990) *Finding Groups in Data? An Introduction to Cluster Analysis*, pp. 69–119, Wiley, New York
28. Miyamoto, S., Akiyama, S. K., and Yamada, K. M. (1995) *Science* **267,** 883–885
29. Visscher, K., Gross, S. P., and Block, S. M. (1996) *IEEE J. Select. Top. Quant. Electr.* **2,** 1066–1076
30. Hynes, R. O. (1992) *Cell* **69,** 11–25
31. Hynes, R. O. (2002) *Cell* **110,** 673–687
32. Gergely, C., Voegel, J., Schaaf, P., Senger, B., Maaloum, M., Horber, J. K., and Hemmerle, J. (2000) *Proc. Natl. Acad. Sci. U. S. A.* **97,** 10802–10807
33. Sagvolden, G. (1999) *Biophys. J.* **77,** 526–532
34. Sung, K. L., Frojmovic, M. M., O'Toole, T. E., Zhu, C., Ginsberg, M. H., and Chien, S. (1993) *Blood* **81,** 419–423
35. Arya, M., Lopez, J. A., Romo, G. M., Cruz, M. A., Kasirer-Friede, A., Shattil, S. J., and Anvari, B. (2003) *Thromb. Haemostasis* **1,** 1150–1157
36. Arya, M., Kolomeisky, A. B., Romo, G. M., Cruz, M. A., Lopez, J. A., and Anvari, B. (2005) *Biophys. J.* **88,** 4391–4401
37. Gottschalk, K. E., Adams, P. D., Brunger, A. T., and Kessler, H. (2002) *Protein Sci.* **11,** 1800–1812
38. Bazzoni, G., and Hemler, M. E. (1998) *Trends Biochem. Sci.* **23,** 30–34
39. Zhang, X. A., Bontrager, A. L., Stipp, C. S., Kraeft, S. K., Bazzoni, G., Chen, L. B., and Hemler, M. E. (2001) *Mol. Biol. Cell* **12,** 351–365
40. Brakebusch, C., and Fassler, R. (2003) *EMBO J.* **22,** 2324–2333
41. DeMali, K. A., Wennerberg, K., and Burridge, K. (2003) *Curr. Opin. Cell Biol.* **15,** 572–582